Materials and Structures, 1993, **26**, 486–494

Micromechanics of crack bridging in fibre-reinforced concrete

V. C. LI

Advanced Civil Engineering Materials Research Laboratory, Department of Civil and Environmental Engineering, University of Michigan, Ann Arbor, MI 48109-2125, USA

H. STANG, H. KRENCHEL

Department of Structural Engineering, Technical University of Denmark, DK 2800, Lyngby, Denmark

The stress–crack width relationship has been determined experimentally for concretes reinforced with two types of fibres, steel and polypropylene, of various fibre volume fractions. A micromechanics-based theoretical model is proposed which captures the essential features of the stress–crack width relationships at small crack widths (less than 0.3 mm). Micromechanisms accounted for include the bridging actions due to aggregates and fibres, Cook–Gordon interface debonding and fibre pre-stress. The fibre bridging action involves interface slip-dependent friction as well as snubbing friction for fibres bridging at inclined angles. Theoretical predictions based on independent parametric inputs compare favourably with experimental measurements of the stress–crack width relationship. Findings in this research provide confidence in the use of the proposed model for materials engineering targeted at prescribed structural performance.

1. INTRODUCTION

Crack width control is of primary importance in many reinforced concrete structures, since it is believed that there is a close relationship between mean or maximum crack widths and the durability of the structure. Furthermore, when the concrete structure in question acts as a containment vessel for fluids, leakage must be minimized or might not be tolerated at all. Consequently, in the serviceability limit state a mean or maximum crack width less than about 0.1–0.3 mm is usually prescribed.

It has been found [1] that there is a close relationship between the tensile load capacity of the concrete cracks (the so-called stress–crack width relationship) and the crack widths for a given loading on a given concrete structure. Furthermore, the ultimate load-carrying capacity of a cracked unreinforced concrete structure was found to depend on the tensile load capacity across the cracks, especially at small crack widths (e.g. [2]). For these reasons the stress–crack width relationship for small crack widths (less than about 0.1–0.3 mm) is of fundamental importance in concrete structure design in both serviceability and ultimate limit state. For example, control of the stress–crack width relationship can reduce the amount of conventional reinforcement and therefore reduce labour costs for a given acceptable crack width [3].

In plain concrete, crack bridging is provided by aggregate locking action. Although the detailed physics has not been fully understood in quantitative terms, aggregate bridging action can be well represented analytically [3]. When fibres are added to concrete, an additional bridging action is brought into effect, superimposing on the aggregate bridging effect. The combined bridging action in a fibre-reinforced concrete (FRC) can be very beneficial to increase the stress carried across the crack. In addition, fibres have been added to concrete to create pseudo-strain-hardening [4,5]. The load transfer capacity across a matrix crack is critical in determining the amount of fibres necessary in achieving pseudo-strain-hardening.

In this paper, the post-cracking stress–crack width relationship (σ_c–w) of the composite is studied from a micromechanics point of view, particularly with reference to fibre bridging action combined with the well-known Cook–Gordon debonding effect [6]. In addition, fibre pre-stressing and slip-dependent interfacial bond strength are accounted for in the model. Analytical results are used to predict stress–crack width relationships for steel fibre and polypropylene fibre reinforced concretes, for various fibre volume fractions. Comparisons between model predictions and experimentally measured σ_c–w relations confirm many of the salient features in the σ_c–w curves associated with the various micromechanisms. A companion paper [7] will describe the use of the proposed analytical model in design and structural applications of fibre-reinforced concrete.

2. CRACK BRIDGING MODEL

2.1 Aggregate bridging action

The post-peak tension-softening of concrete has been modelled as the coalescence of regularly spaced micro-cracks [8–10]. Although these models are convenient to use, the lack of correspondence between the real physical structure of concrete and that of the model makes it difficult to determine physical parameters. For lack of a

0025-5432/93

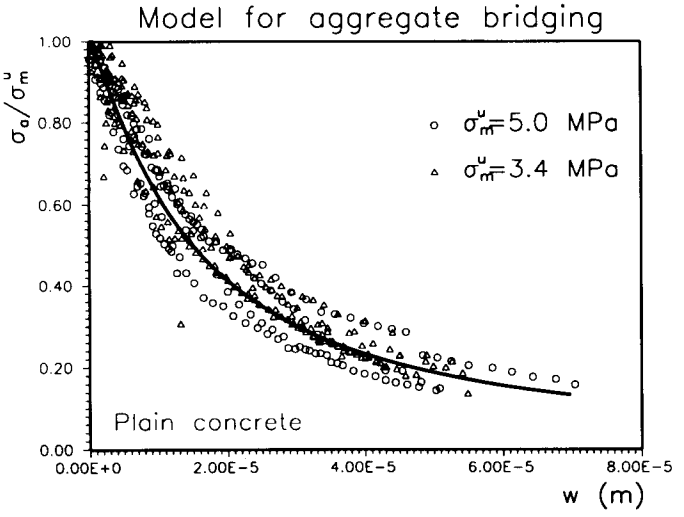

Fig. 1 Post-crack σ_a–w relation for unreinforced concrete (maximum aggregate size = 8 mm) shown together with a fitted curve based on Equation 1. Experimental data include both the normal-strength concrete used in the polypropylene FRC series (σ_m^u = 3.4 MPa) and the high-strength concrete (σ_m^u = 5.0 MPa) used in the steel FRC series.

good physical model, we shall adopt here an empirical model proposed by Stang [1] and which fits a wide range of experimental data extremely well. In this model the aggregate bridging stress σ_a is expressed as a function of the crack opening w:

$$\sigma_a = \frac{\sigma_m^u}{1 + (w/w_0)^p} \tag{1}$$

where σ_m^u is the maximum bridging stress due to aggregate action at $w = 0$. The parameter p describes the shape of the softening process with increasing crack opening, and has been determined to be close to unity for most concrete tested to date. The parameter w_0 corresponds to the crack opening when the stress has dropped to half of σ_m^u. Equation 1 is shown in Fig. 1 with $p = 1.2$ and $w_0 = 0.015$ mm. Two concrete types with a maximum aggregate size of 8 mm were used in the fibre-reinforced concretes. The one reinforced with polypropylene fibres is a normal-strength concrete with $\sigma_m^u = 3.4$ MPa, whereas the one reinforced with steel fibres is a high-strength concrete with $\sigma_m^u = 5.0$ MPa. Equation 1 is shown to describe the two concretes very well, at least for the range of w indicated ($w \leq 0.07$ mm).

2.2 Fibre bridging action

Based on the concept of debonding against a frictional strength of τ and on the concept of an inclined fibre acting as a flexible rope passing over a frictional pulley against a snubbing coefficient f [11], Li [12] derived the fibre bridging stress by integrating the individual contribution of fibres located at various centroidal distances (z) from the matrix crack and at various orientations (ϕ) relative to the tensile loading direction. For a composite with fibre volume fraction V_f of fibres of length L_f and diameter d_f, the bridging stress σ_f may be expressed as a function of cracking opening δ:

$$\sigma_f(\delta) = \frac{4V_f}{\pi d_f^2} \int_{\phi=0}^{\pi/2} \int_{z=0}^{(L_f/2)\cos\phi} P(\delta)p(\phi)p(z)\, dz\, d\phi \tag{2}$$

where $P(\delta)$ is the bridging force exerted by a single fibre with an embedded length (the shorter of the two on either side of the matrix crack) of l at an orientation angle ϕ:

$$P(\delta) = \frac{\pi}{2}[(1+\eta)E_f d_f^3 \tau\delta]^{1/2} e^{f\phi} \quad \text{for} \quad \delta \leq \delta_0 \tag{3a}$$

$$P(\delta) = \pi\tau l d_f\left(1 - \frac{\delta - \delta_0}{l}\right) e^{f\phi} \quad \text{for} \quad \delta_0 < \delta \leq \delta_0 + l \tag{3b}$$

$$P(\delta) = 0 \quad \text{for} \quad \delta_0 + l \leq \delta \tag{3c}$$

where $\delta_0 \equiv 4l^2\tau/[(1+\eta)E_f d_f]$ and $\eta \equiv V_f E_f / V_m E_m$. In the above, E_m and V_m stands respectively for the Young's modulus and volume fraction of the matrix material which contains the fibres, and E_f stands for the Young's modulus of the fibre.

Substitution of Equations 3 into Equation 2 and assuming three-dimensional uniform randomness for the probability density functions $p(\phi)$ and $p(z)$ gives the pre-peak fibre bridging stress [12]:

$$\sigma_f(\tilde{\delta}) = \sigma_0\left[2\left(\frac{\tilde{\delta}}{\tilde{\delta}^*}\right)^{1/2} - \frac{\tilde{\delta}}{\tilde{\delta}^*}\right] \quad \text{for} \quad 0 \leq \tilde{\delta} \leq \delta^* \tag{4}$$

where $\sigma_0 \equiv g\tau V_f(L_f/d_f)/2$, $\tilde{\delta} \equiv \delta/(L_f/2)$, and where

$$\tilde{\delta}^* \equiv \frac{2\tau}{(1+\eta)E_f}\left(\frac{L_f}{d_f}\right)$$

corresponds to the maximum attainable value of δ_0 (normalized by $L_f/2$) for the fibre with the longest possible embedment length of $L_f/2$. The snubbing factor g in Equation 4 is defined in terms of the snubbing coefficient f:

$$g \equiv \frac{2}{4 + f^2}(1 + e^{\pi f/2}) \tag{5}$$

The post-peak stress versus crack opening relationship can be derived from Equation 2 by using only Equation 3b and the result is [12]

$$\sigma_f(\tilde{\delta}) = \sigma_0[1 - (\tilde{\delta} - \tilde{\delta}^*)]^2 \quad \text{for} \quad \tilde{\delta}^* < \tilde{\delta} \leq 1 \tag{6}$$

Equation 6 has been found to compare favourably with experimental data for both steel and polymeric FRC materials [12].

In deriving Equations 4 and 6, care must be taken to discount the contribution of those fibres which have slipped out of the matrix. This amounts to eliminating those fibres whose embedment length l is less than the crack opening δ in the integration process in Equation 2, as specified in Equations 3.

In the event that the interfacial bond hardens with slip distance [13] or weakens with slip distance [13–15], τ may be expressed as a function of local slippage δ'.

A convenient polynomial form has been employed previously and appears to describe the experimental data for fibre pull-out reasonably well:

$$\tau(\delta') = \tau_0 + a_1\delta' + a_2(\delta')^2 \tag{7}$$

The constants τ_0, a_1 and a_2 must be experimentally determined for each specific combination of fibre type, matrix, and processing conditions. Because the local slippage prior to complete debonding is typically very small, it would be useful to simplify Equation 7 by equating δ to δ', so that the local slippage is assumed to be equal to the fibre end slippage after complete debonding. Thus Equation 7 should be rewritten as

$$\begin{aligned} \tau(\delta) &= \tau_0 && \text{for} \quad \delta \leq \delta^* \\ \tau(\delta) &= \tau_0 + a_1\delta + a_2\delta^2 && \text{for} \quad \delta > \delta^* \end{aligned} \tag{8}$$

We now consider the additional bridging compliance as a result of the Cook–Gordon effect. Cook and Gordon [6] predicted that a crack of finite root radius in an elastic solid under remote tensile load will create a crack tip stress field with a crack-plane-parallel tensile component which reaches a maximum at a distance of the radius of the crack tip. Thus a matrix crack approaching an isolated fibre can cause interface debonding before the crack tip reaches the fibre–matrix interface if the interfacial strength is adequately weak. This Cook–Gordon effect is illustrated schematically in Fig. 2. Interfacial debonding has been identified by SEM observations in fibre-reinforced ceramics to act as local events precursory to first cracking [16]. Direct observation [17,18] of the Cook–Gordon effect by means of *in situ* SEM, in a steel fibre-reinforced cement paste, suggests that the debond zone can extend for 200 μm to over 1000 μm, and is likely to depend on the inhomogeneity of the interfacial microstructure. As a consequence, we expected an additional displacement δ_{cg} related to the elastic stretching of the debonded length α, hereafter labelled as the Cook–Gordon parameter. For a single fibre, the additional displacement may be estimated as follows:

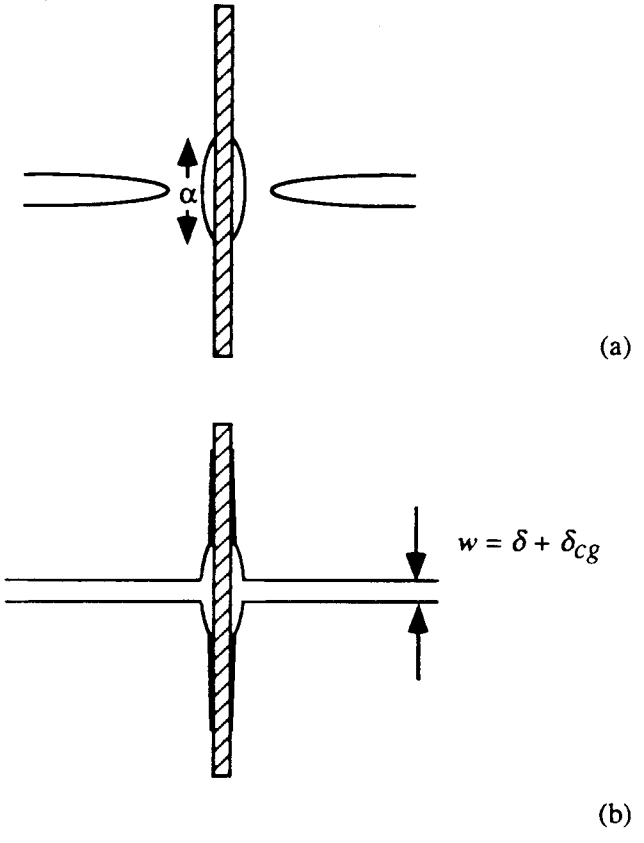

Fig. 2 The Cook–Gordon effect (a) induces fibre–matrix separation due to the tensile stress in the horizontal direction associated with the elastic crack tip field of the approaching matrix crack, and (b) leads to an additional crack opening δ_{cg} due to elastic stretching of the fibre segment α in addition to that δ associated with interface frictional debonding.

$$\delta_{cg} = \frac{4\alpha P}{\pi d_f^2 E_f} \tag{9}$$

This P–δ relationship for a single fibre may be substituted into Equation 2 to obtain

$$\delta_{cg} = \frac{4\alpha}{V_f E_f}\sigma_f \tag{10}$$

so that the total crack width w is approximately given as

$$w = \delta + \delta_{cg} \tag{11}$$

with δ related to σ_f by Equations 4 and 6, and δ_{cg} given by Equation 10 above. This procedure allows us to calculate the fibre bridging stress σ_f indirectly as a function of the total crack width w.

Finally, it should be recognized that at the formation of a matrix crack, and prior to any crack opening, the fibre is already in a stressed state. The level of pre-stressing σ_{ps}^0 may be estimated from the load-sharing between fibre and matrix at the matrix cracking strain. This leads to [19]

$$\sigma_{ps}^0 = \eta_\theta \eta_l \varepsilon_{mu} E_f V_f \tag{12}$$

where ε_{mu} is the matrix cracking strain, typically around 0.02% for cementitious materials, and η_θ and η_l are orientation and length efficiency factors, respectively. For a three-dimensional uniform random distribution of fibres, Cox [20] found that $\eta_\theta = 1/6$ for unconstrained deformation, and Krenchel [21] found that $\eta_\theta = 1/5$ for the case when deformation is constrained to the direction of applied tensile loading. For the present purpose, since we intend to use Equation 12 for the post-crack contribution of fibres, and since in this stage all bridging fibre segments crossing the matrix crack will be reorientated along the load direction, it would seem appropriate to employ $\eta_\theta = 1$. For the efficiency factor related to finite fibre length, based on the assumption of an elastic bond, Laws [22] found that η_l may be expressed in the following form:

$$\eta_l = 1 - \frac{\varepsilon_{mu} E_f d_f}{4 L_f \tau_0} \tag{13}$$

Fibre prestressing may be expected to be reduced by the interfacial debonding process, and the prestress should be completely eliminated when the fibre is fully debonded. This occurs when δ has reached δ^*. As a first approximation, we assume that the prestress level diminishes linearly with crack opening, so that

$$\begin{aligned} \sigma_{ps}(w) &= \sigma_{ps}^0(w^* - w)/w^* \quad \text{for} \quad w < w^* \\ \sigma_{ps}(w) &= 0 \quad \text{for} \quad w \geq w^* \end{aligned} \tag{14}$$

where

$$w^* = \delta^* + \delta_{cg}(\sigma_f = \sigma_0) \tag{15}$$

In a fibre-reinforced concrete, and especially for a small crack opening, the aggregate bridging effect and the fibre bridging effect may be assumed to operate simultaneously. When the prestressing effect is included, the total composite bridging stress $\sigma_c(w)$ is then given by

$$\sigma_c(w) = \sigma_a(w) + \sigma_f(w) + \sigma_{ps}(w) \tag{16}$$

with $\sigma_a(w)$ as given by Equation 1 and $\sigma_f(w)$ and $\rho_{ps}(w)$ as just described. Equation 16 is used to predict composite bridging stress as a function of crack opening for two families of FRCs to be described below.

3. EXPERIMENTAL DETERMINATION OF STRESS–CRACK WIDTH RELATIONSHIP

In order to determine the stress–crack width relationship experimentally, deformation-controlled tensile tests were conducted on notched specimens with thickness 40 mm, width 50 mm and height 55 mm. To eliminate the prestressing inevitably introduced in the specimens when using conventional grips, for improved alignment, and for maximum stiffness, a special specimen fixture was developed. This fixture consists of two interchangeable steel blocks on to which the specimens were glued. The steel blocks were both fixed in advance to the frame and the crosshead of a 100 kN 6025 Instron testing machine equipped for closed-loop testing.

The deformation was measured using two standard Instron extensometers (type 2620-602) with 12.5 mm gauge length mounted across each of the two 10 mm deep and 3 mm wide notches. The test was conducted as a prescribed deformation-rate test using the average signal from the extensometer as feedback. An initial crosshead rate of 1.25×10^{-3} mm min^{-1} was used. After the peak was reached the rate was slowly increased to 6.25×10^{-2} mm min^{-1}.

The experimental set-up is shown in Fig. 3. Technical details on testing procedure and type of adhesion used can be found elsewhere [14].

The raw data consisted of time, load, displacement reading from each extensometer, and average displacement. Data were recorded by the testing machine and transferred to a PC. The crack opening was extracted from the total average displacement across the crack by subtracting the total elastic and inelastic deformation outside the crack. This was done by assuming that the material outside the crack unloaded linearly with a stiffness corresponding to the initial stiffness observed in uniaxial tension (see e.g. [23,24]).

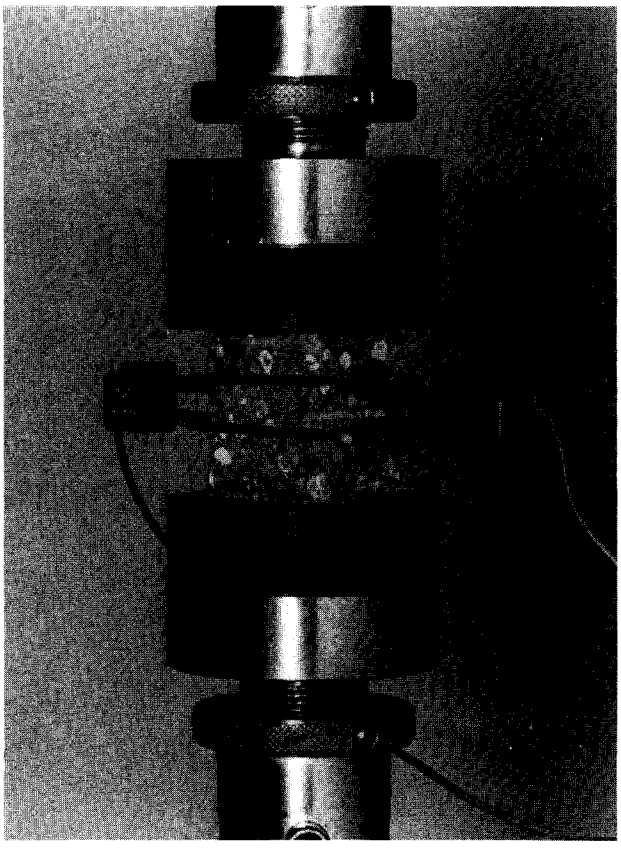

Fig. 3 Set-up for the uniaxial tension test of FRC.

The stress–crack width relationship was determined experimentally on two sets of FRC materials: polypropylene fibres in normal-strength concrete and steel fibres in high-strength concrete. Details of recipes, mixing procedures and curing can be found elsewhere for the polypropylene fibre FRC [25] and the steel fibre FRC [26]. The maximum aggregate size was 8 mm in both concretes.

4. COMPARISON BETWEEN MODEL PREDICTION AND EXPERIMENTAL DATA

4.1 Independently measured or deduced parameters

The aggregate bridging parameters $p = 1.2$ and $w_0 = 0.015$ mm have been obtained by fitting Equation 1 to experimental σ_a–w curves obtained with the two concrete matrices, as shown in Fig. 1. The ultimate aggregate bridging stress σ_m^u has been obtained directly from the peak uniaxial tensile load of these matrices. For the normal-strength $\sigma_m^u = 3.4$ MPa and for the high-strength concrete $\sigma_m^u = 5.0$ MPa. The same normal-strength concrete matrix has been used in all the polypropylene FRC samples, and the same high-strength concrete matrix has been used in all the steel FRC ones. We make the assumption that the aggregate bridging parameters are

Table 1 Fibre and interfacial parametric values used as model input

Fibre types	Fibre parameters			Interfacial parameters				
	E_f (GPa)	L_f (mm)	d_f (mm)	τ_0 (MPa)	a_1 (MPa mm^{-1})	a_2 (MPa mm^{-1})	f	α (mm)
Steel	210	25	0.4	4.2	−4.0	1.0	0.75	6.0
Polypropylene	11.9	12	0.048	0.8	0	0	0	0.72

not affected by the presence of the low volume of fibres used in the present study.

The only other concrete matrix parameter needed in the calculation of fibre prestressing level (Equation 12) is the failure strain ε_{mu}, which we again assume not to be affected by the presence of the low volume of fibres used in present series of tests. Assuming a linear response up to failure, we use here

$$\varepsilon_{mu} = \frac{\sigma_m^u}{E_m} \tag{17}$$

where E_m has been determined from the initial slope of the tensile stress–strain curve. For both matrices $E_m \simeq 30$ GPa, so that ε_{mu} for the normal-strength concrete is 0.013% and that for the high-strength concrete is 0.017%.

All fibre parameters E_f, L_f and d_f are measurable with good accuracy. Values for these parameters for the steel fibres and polypropylene fibres used can be found in Table 1. We note here that the polypropylene fibre used has a rectangular cross-section, and an effective fibre diameter has been employed:

$$d_f = \frac{2bt}{b+t} \tag{18}$$

where b and t are the width and thickness of the fibre. Equation 18 has taken into account the change in surface contact area per fibre and the change in the number of fibres due to the rectangular cross-section for a given fibre volume fraction.

The interfacial parameters required in the model consist of the interfacial bond strength τ as expressed in Equation 7, the snubbing coefficient f, and the Cook–Gordon parameter α. We discuss each of these parameters in the following.

The slip-dependent bond strength has been measured by Glavind [15] for steel fibre by means of pull-out tests. Both the fibre and the concrete matrix were similar to those used in the present experiment. The results reported [15] show quite large variations in the bond parameters for relatively small variations in matrix composition. The values used here, as shown in Table 1, are of the same order of magnitude as the parameters reported previously [15]. There are no similar measurements available for the polypropylene fibres, although slip hardening has been previously reported [13] in a polyethylene fibre. We have assumed here that the bond strength remains constant at τ_0. From an independent test series employing continuous aligned fibres of the same kind, Stang [27] inferred τ_0 to be in the range of 0.4 to 1.8 MPa, based on the bend-over point of the uniaxial stress–strain curve and on an analytical model originated by Aveston *et al.* [28]. Because the aligned fibre specimens employ an extremely well-packed neat cement matrix processed by a pultrusion technique, we expect the actual bond strength for the present FRCs (with short random fibres) processed by conventional vibration casting to be in the low end of this range. A value of 0.8 MPa has been adopted for use in the present model.

The snubbing coefficient f for steel fibres in a concrete matrix has been studied by Li *et al.* [11]. They inferred from the maximum post-peak stress of a test series by Visalvanich and Naaman [29] that f lies somewhere between 0.5 and 1.0. An average value of 0.75 has been adopted for the present model. No corresponding data exist for polypropylene fibre, and $f = 0$ has been assumed for this type of fibre.

Finally, the Cook–Gordon parameter α presents the greatest uncertainty. It would seem not unreasonable to gauge its value from the magnitude of the distance between adjoining cracks observed to zig-zag at fibre sites [17], which would suggest that α should fall in the range of one to several tens of the fibre diameter. Bentur [40] has suggested $\alpha = 2d_f - 10d_f$ for steel fibre in neat cement paste. For steel fibre in a more heterogeneous concrete matrix, we may expect larger values of α. We have adopted $\alpha = 15d_f$ for lack of more precise experimental evidence.

4.2 Model results

Fig. 4a–e shows the predicted σ_c–w curves for the steel FRC with $V_f = 0$, 0.5, 1.0, 1.5 and 2.0%, respectively, together with the experimental data obtained from the uniaxial test procedure described in section 3. In all five plots, the fibre and concrete matrix data for model input are fixed as described above in the section 4.1. Only the fibre volume is changed. The 0% data and curve are included to show that the model remains valid even when the fibre volume fraction approaches zero. In both experimental data and theoretical predictions, these σ_c–w curves are characterized by an initial load drop followed by a stress rise and a subsequent close to linear decay. The maximum stress at $w = 0$ increases by a small amount, with a weak dependence on V_f. The magnitude

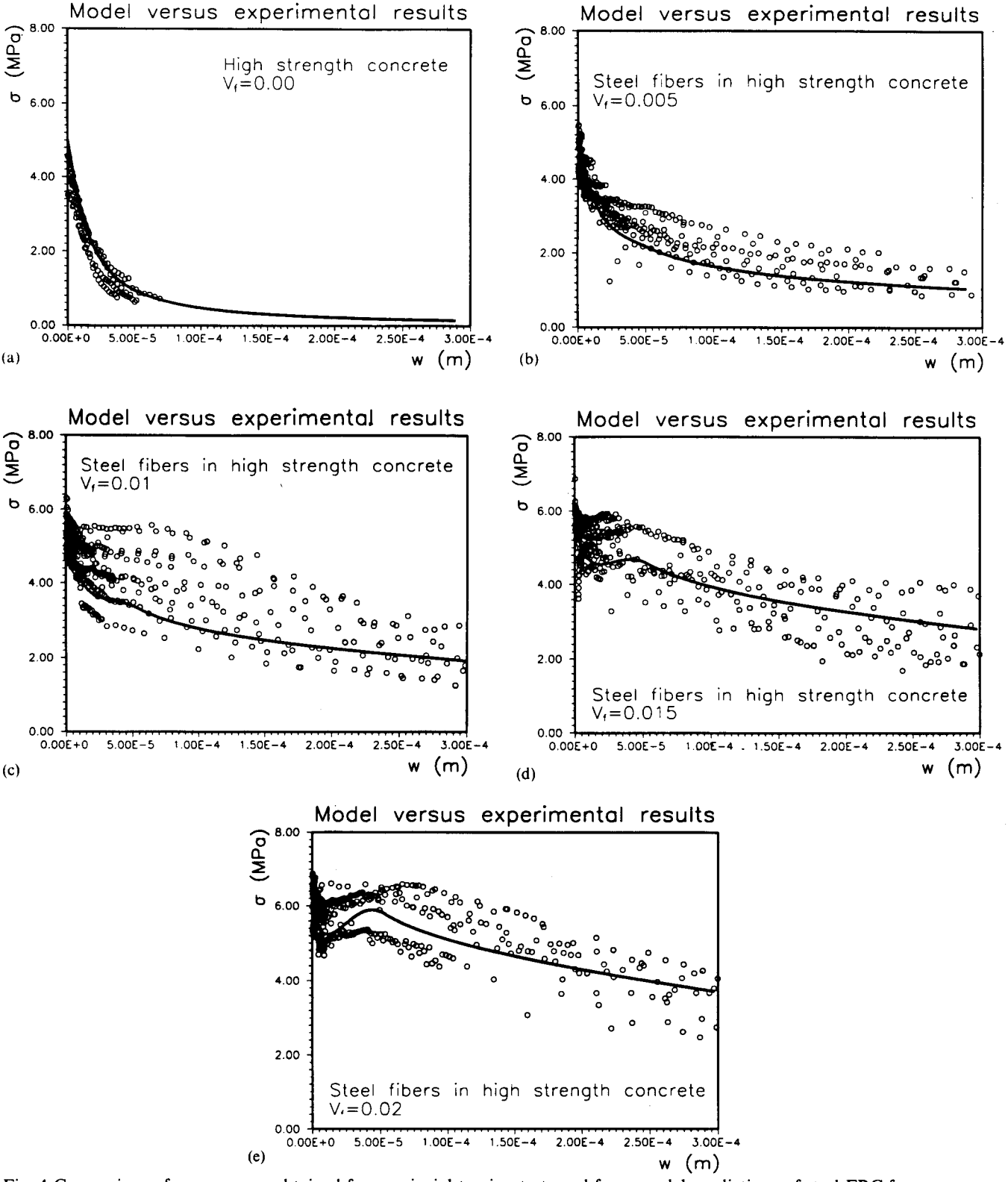

Fig. 4 Comparison of σ_c–w curves obtained from uniaxial tension tests and from model predictions of steel FRC for (a) $V_f = 0.0$, (b) $V_f = 0.5$, (c) $V_f = 1.0$, (d) $V_f = 1.5$ and (e) $V_f = 2.0\%$.

of the bumps for very small crack widths appears accentuated by increasing fibre volume fractions.

Fig. 5a–d shows a similar set of data, but for polypropylene FRC. The fibre volume percentages are 0.0, 1.0, 2.0 and 3.0, respectively. The general trend both experimental and theoretical, of the σ_c–w curves indicates a smoother decay in comparison to those of steel fibre-reinforced concrete. Again, the parametric values used in the model are fixed and described in the previous section, and only the fibre volume fraction is changed for model input for these figures.

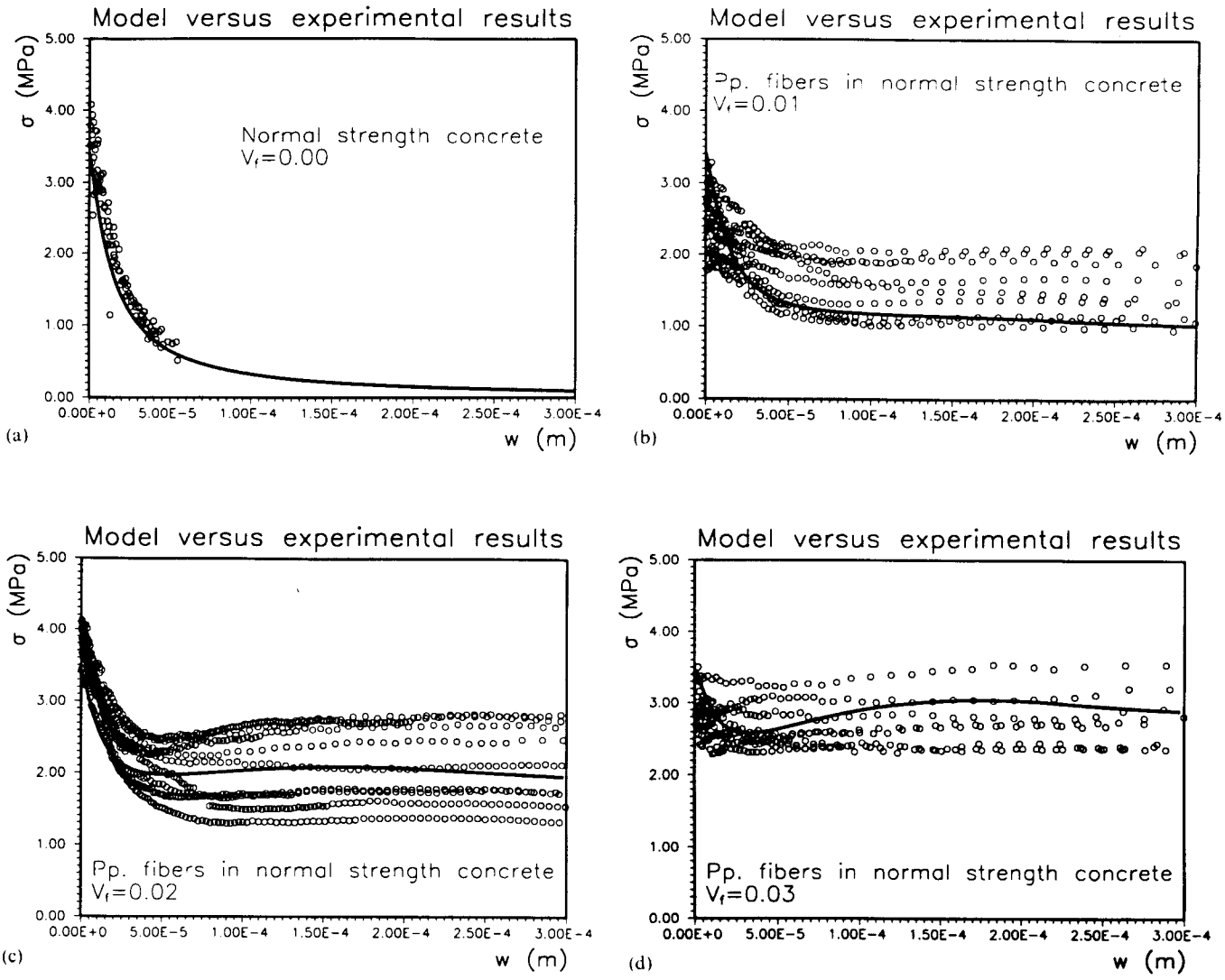

Fig. 5 Comparison of σ_c–w curves obtained from uniaxial tension tests and from model predictions of polypropylene FRC for (a) $V_f = 0.0$, (b) $V_f = 1.0$, (c) $V_f = 2.0$ and (d) $V_f = 3.0\%$.

5. DISCUSSION OF MECHANISMS GOVERNING THE σ_c–w CURVES

To gain physical insight into the governing mechanisms of the σ_c–w curves, we have separately plotted in Fig. 6 the individual contributions of the aggregate bridging action, the fibre bridging action and the fibre prestress (using $V_f = 2\%$ steel fibre as illustration), represented by Equations 1, 4, 6 and 14, respectively. These three bridging actions control the broad picture of the shape of the σ_c–w curves. Indeed, the major difference between the σ_c–w relations of steel and polypropylene FRCs lies in the fibre bridging action, as expected, and Fig. 6 indicates that the elastic modulus of the fibre dominates the location of the peak (at δ^*) in the fibre bridging action. Thus, the stiffer steel fibres create a stronger bump in the σ_c–w curve, at smaller crack opening due to the smaller δ^*. The more gentle fibre bridging action of the lower-modulus polypropylene fibres in turn explains the smoother σ_c–w curves observed when testing the corresponding FRC. The prestressing mechanism is

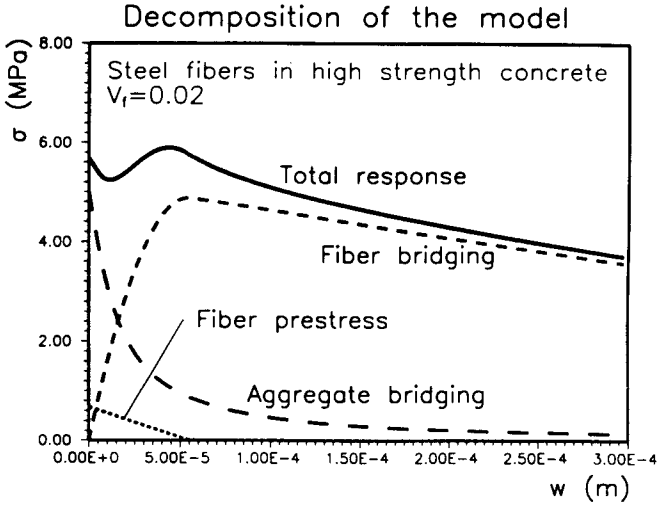

Fig. 6 Individual contributions of aggregate bridging action and fibre bridging action to σ_c–w curves. Illustrated also is the fibre pre-stressing effect. Steel fibres in high-strength concrete, $V_f = 2.0\%$.

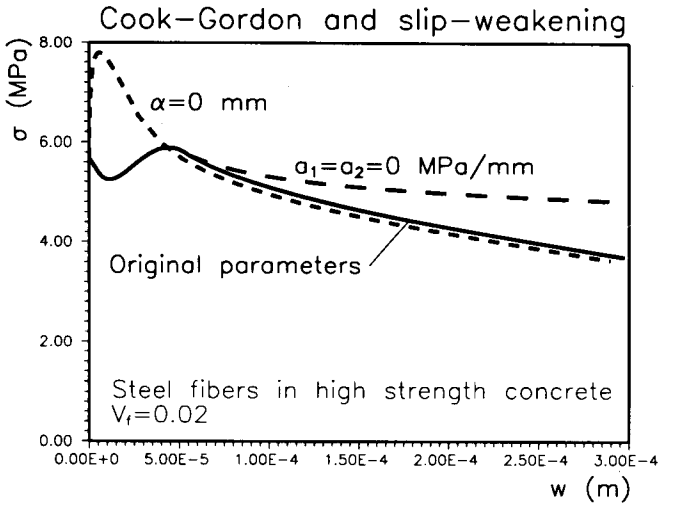

Fig. 7 Influence of Cook–Gordon effect on the σ_c–w curves. Friction bond decay is also illustrated. Steel fibres in high-strength concrete; $V_f = 2.0\%$.

responsible for the definite, albeit small, tensile strength increase with steel fibre volume fraction at $w = 0$.

Fig. 7 shows the combined influence of aggregate bridging and fibre bridging, with and without the Cook–Gordon effect. It is clear that when the Cook–Gordon effect is absent, the overestimated initial fibre bridging stiffness causes a rise in the curve at $w \simeq 0$ which is not observed in any of the experimental data sets. Thus the Cook–Gordon effect of an initial debonded segment is indirectly revealed in the σ_c–w measurements. The influence of frictional bond decay with slippage (Equation 7) is also illustrated.

6. CONCLUSION

We have presented a micromechanically based analytical model which describes the post-crack bridging stress–crack width relationship in FRC materials. This relationship is best summed up in the following form:

$$\sigma_c = F(w, \text{concrete parameters, fibre parameters, interface parameters}) \quad (19)$$

where the concrete parameters consist of E_m, σ_m^u, p and w_0, the fibre parameters consist of V_f, E_f, L_f and d_f, and the interface parameters consist of τ, f and α. Armed with these constituent material parameters, the composite σ_c–w relationship, highly non-linear as it may be, can be easily calculated so long as the assumptions built into the model are satisfied. With two highly different fibre types, steel and polymer, as reinforcements for a concrete composite, and with four and three different fibre volume fractions each, Figs 4 and 5 demonstrate that the proposed model can be applied with some confidence. Equation 19 implies that this important composite property can be engineered by controlling the concrete, fibre and interface parameters, so that a composite with the desirable σ_c–w relationship can be designed.

Another application of the present model, embodied in the form of Equation 19, is in the design or prediction of structural response, when the material is a fibre-reinforced concrete without pseudo-strain-hardening. At present, a constraining factor in the application of fibre-reinforced concrete to practical structures is the lack of design tools to allow the structural engineer to predict the structural response. For this purpose, Equation 19 serves as a constitutive relation, similar to those currently used in governing the elastic or non-linear elastic behaviour of concrete, but specialized for handling the post-crack regime in a fibre-reinforced concrete structure. Further, as alluded to in section 1, for the purpose of leakage control in fluid-containing concrete vessels, or in durability design for general concrete structures, particularly those exposed to aggressive environments such as in coastal regions or parking decks, crack width control will be paramount in maintaining structural functionality. Again, Equation 19, in combination with finite-element analysis, would serve as an analytical tool for crack width control, to be carried out *before* the structure is built and put into service.

Micromechanical models such as Equation 19 allow the structural designer and/or materials engineer to choose an appropriate materials receipe which will best meet the required structural performance.

ACKNOWLEDGEMENTS

This work was performed while Victor C. Li was a Visiting Professor at the Department of Structural Engineering at The Technical University of Denmark (DTH) in June–August, 1992. Funding by DTH for the Visiting Professorship is gratefully acknowledged. V. C. Li would like to thank his colleagues at DTH for their hospitality and cooperation during his stay in Denmark. Dr Henrik Stang and Professor Herbert Krenchel acknowledge support from the Research Programme on Fibre Reinforced Cementitious Composites sponsored by The Danish Council for Scientific and Industrial Research and The Danish Ministry for Industry. Discussions with Arnon Bentur have been particularly helpful with regard to the Cook–Gordon effect.

REFERENCES

1. Stang, H., 'Evaluation of properties of cementitious materials', in 'High Performance Fiber Reinforced Cement Composites', Proceedings of International RILEM/ACI Workshop, edited by H. W. Reinhardt and A. E. Naaman (Spon, 1992) pp. 388–406.
2. Li, V. C. and Liang, E., 'Fracture processes in concrete and fibre-reinforced cementitious composites', *ASCE J. Eng. Mech.* **12**(6) (1986) 566–586.
3. Stang, H. and Aarre, T., 'Evaluation of crack width in FRC with conventional reinforcement' *J. Cem. Concr. Compos.* **14**(2) (1992) 143–154.
4. Li, V. C. and Wu, H. C., 'Conditions for pseudo strain-hardening in fiber reinforced brittle matrix composites', *J. Appl. Mech. Rev.* **45**(8) (1992) 390–398.
5. Li, V. C. and Leung, C. K. Y., 'Theory of steady state and

multiple cracking of random discontinuous fiber reinforced brittle matrix composites', *ASCE J. Engng Mech.* **118**(11) (1992) 2246–2264.
6. Cook, J. and Gordon, J. E., 'A mechanism for the control of crack propagation in all brittle systems', *Proc. Roy. Soc.* **282A** (1964) 508–520.
7. Stang, H., Li, V. C. and Krenchel, H., 'Design and structural applications of stress–crack width relations in fiber reinforced concrete', in preparation.
8. Ortiz, M., 'Microcrack coalescence and macroscopic crack growth initiation in brittle solids', *Int. J. Solids Struct.* **24** (1988) 231–250.
9. Horii, H., Hasegawa, A. and Nishino, F., 'Fracture process and bridging zone model and influencing factors in fracture of concrete', in 'Fracture of Concrete and Rock', edited by S. P. Shah and S. E. Swartz (Springer, New York, 1989), pp. 205–219.
10. Karihaloo, B. L. and Huang, X., 'Tensile response of quasi-brittle materials', *Pure Appl. Geophys.* **137**(4) (1991) 461– 427.
11. Li, V. C. Wang, Y. and Backer, S., 'Effect of inclining angle, bundling, and surface treatment on synthetic fiber pull-out from a cement matrix', *J. Compos.* **21**(2) (1990) 132–140.
12. Li, V. C., 'Post-crack scaling relations for fiber reinforced cementitious composites', *ASCE J. Mater. Civil Engng* **4**(1), (1992) 41–57.
13. Wang, Y., Li, V. C. and Backer, S., 'Modeling of fiber pull-out from a cement matrix', *Int. J. Cem. Compos. Lightwt Concr.* **10**(3) (1988) 143–149.
14. Aarre, T., 'Tensile Characteristics of FRC with Special Emphasis on its Applicability in a Continuous Pavement', PhD thesis, Department of Structural Engineering, Technical University of Denmark (1992).
15. Glavind, M., 'Evaluation of the Compressive Behavior of Fiber Reinforced High Strength Concrete', PhD thesis, Department of Structural Engineering, Technical University of Denmark (1992).
16. Barsoum, M. W., Kangutkar, P. and Wang, A. S. D., 'Matrix crack initiation in ceramic matrix composites. Part I: Experiments and test results', *Compos. Sci. Technol.* **44** (1992) 257–269.
17. Bentur, A., Diamond, S. and Mindess, S., 'Cracking process in steel fiber reinforced cement paste', *Cem. Concr. Res.* **15** (1985) 331–342.
18. *Idem*, 'The microstructure of steel fiber–cement interface', *J. Mater. Sci.* **20** (1985) 3610–3620.
19. Bentur, A. and Mindess, S., 'Fiber Reinforced Cementitious Composites' (Elsevier Applied Science, 1990) p. 449.
20. Cox, H. L., 'The elasticity and strength of paper and other fibrous materials', *Br. J. Appl. Phys.* **3** (1952) 72–79.
21. Krenchel, H., 'Fibre Reinforcement' (Akademisk, Copenhagen, 1964) p. 159.
22. Laws, V., 'The efficiency of fibrous reinforcement of brittle matrices', *J. Phys. D: Appl. Phys.* **4** (1971) 1737–1746.
23. Hordijk, D. A., Van Mier, J. G. M. and Reinhardt, H. W., 'Material properties', in 'Fracture Mechanics of Concrete Structures, From Theory to Applications', edited by L. Elfgren (Chapman and Hall, London, 1991) pp. 67–127.
24. Petersson, P.-E., 'Crack Growth and Development of Fracture Zones in Plain Concrete and Similar Materials'. Report TVBM-1006 (Division of Building Materials, Lund Institute of Technology, 1981).
25. Hansen, S. and Stang, H., 'Experimentally Determined Mechanical Properties for Fiber Concrete' (Report Series R, No. 305, Department of Structural Engineering, Technical University of Denmark, 1993).
26. Thygesen, E., 'Design of FRC-materials and Structures', PhD thesis, Department of Structural Engineering, Technical University of Denmark (1992) (in preparation, in Danish).
27. Stang, H., 'Indirect determination of interfacial strength parameters', in preparation.
28. Aveston, J., Cooper, G. A. and Kelly, A., 'Single and multiple fracture', in 'Properties of Fiber Composites', Conference Proceedings (IPC Science and Technology, 1971) pp. 15–24.
29. Visalvanish, K. and Naaman, A. E., 'Fracture modelling for fiber reinforced cementitious composites', Program Report for NSF Grant ENG 77-23534 (Department of Materials Engineering, University of Illinois at Chicago Circle, Chicago, 1982).
30. Bentur, A., personal communication.

RESUME

Micromécanique de la reprise de fissurations dans le béton renforcé de fibres

On a déterminé de façon expérimentale la relation contrainte–largeur de fissure pour des bétons renforcés par deux types de fibres – acier et polypropylène – avec différentes proportions en volume de fibres. On propose un modèle théorique basé sur la micromécanique, qui prend en compte les caractéristiques essentielles des relations contrainte–largeur de fissure pour des largeurs limitées (<0,3 mm). Les micromécanismes pris en considération comprennent l'effet de pontage, l'effet Cook–Gordon à l'interface et la précontrainte des fibres. L'effet de pontage des fibres implique un frottement en relation avec le glissement et un frottement qui relève les fibres se croisant à angles obliques. La comparaison entre les prédictions théoriques basées sur des paramétres indépendants et les mesures expérimentales de la relation contrainte–largeur de fissure est satisfaisante. Les résultats de cette recherche donnent confiance dans l'utilisation du modèle proposé pour des matériaux de génie civil destinés à des performances structurelles prescrites.